Journal of Applied Electrochemistry **30**: 1421–1431, 2000.

TiCN and metallic coatings for corrosion protection of separator plates in MCFCs†

M. KEIJZER[1,2,3], K. HEMMES[2], J.H.W. DE WIT[2] and J. SCHOONMAN[3]
[1]*Current address: Netherlands Energy Research Foundation ECN, Westerduinweg 3, 1755, LE Petten, The Netherlands*
[2]*Laboratory for Corrosion Technology, Electrochemistry and Spectroscopy, Delft University of Technology, Rotterdamseweg 137, 2628 AL Delft, The Netherlands*
[3]*Laboratory for Inorganic Chemistry, Delft University of Technology, Julianalaan 136, 2628 BL Delft, The Netherlands*

Received 31 July 1999; accepted in revised form 23 November 1999

Key words: coatings, corrosion, fuel cell, molten carbonate, titanium nitride

Abstract

Stainless steel 304 substrates were coated with different materials in order to find a suitable coating material for corrosion protection of separator plates in molten-carbonate fuel cells (MCFCs). Five titanium carbonitride coatings differing in composition and morphology and a titanium monoxide coating were deposited with chemical vapour deposition techniques. Also double-layer coatings of TiN/Au and TiN/Ni were prepared. The coatings were tested on their corrosion protection of separator plates in four different environments: under MCFC-cathode or anode gas, at load or at open circuit conditions. The corrosion behaviour was characterized using cyclic voltammetry. Corrosion rates were determined with electrochemical methods and cross-section analyses of corrosion layers. Titanium nitride coatings showed the best corrosion protection. The titanium carbide and titanium monoxide coating showed respectively less and no protection. The thin gold and Ni-coatings were unstable. Under cathode gas, the most important corrosion protection is given by keeping the cell at load, and then a titanium nitride coating might provide lifetime protection. Under anode gas, corrosion is most severe at load conditions. A titanium nitride coating also gives corrosion protection, but not enough for lifetime protection.

1. Introduction

Corrosion of the stainless steel separator plates and current collectors is a severe problem in molten-carbonate fuel cells (MCFCs). The separator plates have to separate anode gas from cathode gas and provide electrical contact between cells in combination with the current collectors. Corrosion of the separator plates affects the endurance and performance of the fuel cell by dissolution into the melt and the formation of oxidation products with a low electronic conductivity. The main goal of this study is to develop a coating to protect steel separator plates and current collectors against corrosion in MCFCs. A suitable coating material should be corrosion resistant, electronically conducting, high-temperature resistant, and have an acceptable price. Based on these requirements and some preliminary exposure tests, TiN and TiC were selected as suitable coating materials [1, 2].

In principle, TiN and TiC are not stable in molten carbonates. For Ti-based materials, Li_2TiO_3 is the only thermodynamically stable phase within the electrochemical window of molten carbonates [1–5]. However, especially when the kinetics of the conversion to Li_2TiO_3 is slow, TiN and TiC are much more favourable coating materials than Li_2TiO_3 because of the conductivity demand. The electronic resistance of a thin Li_2TiO_3 layer (6.7 nm) is high enough to cause a significant potential drop (10 mV) at an average current density of 150 mA cm^{-2}, which corresponds to MCFC load-conditions. The electronic resistance of TiN and TiC coatings and the potential drop caused by them are negligible [1, 2]. Furthermore, after surface oxidation of the TiN or TiC, the formed Li_2TiO_3 layer may behave as passive layer and protect the underlying TiN or TiC from further corrosion.

The coating should be non-porous and free from cracks or pinholes, for these allow electrolyte to contact the substrate and cause accelerated substrate corrosion. Dense layers of TiN and TiC are preferably deposited with chemical vapour deposition (CVD). Five TiCN coatings differing in composition and morphology were deposited on stainless steel 304 substrates with thermal and plasma-enhanced CVD. Also a TiO coating was

† Dedicated to the memory of Daniel Simonsson

deposited with thermal CVD to study the conversion to Li_2TiO_3.

Further, two double-layer combinations were prepared by depositing either gold or nickel on TiN-coated steel samples. The gold and nickel coatings may provide the corrosion protection. The intermediate TiN layer may protect the steel substrate against corrosion at cracks, or other defects in the gold or nickel layer, and also function as diffusion barrier for small metal ions such as Fe and Cr from the steel substrate [6]. Nickel is only stable under anode gas conditions, not under cathode gas conditions [2, 7]. The gold coating may provide the corrosion protection under cathode gas conditions, because gold is the only metal which is stable under cathode gas conditions.

These coated samples were tested in molten carbonate, with emphasis on finding a relation between the coating composition, morphology, and corrosion properties, and also in order to find a lifetime corrosion protective coating for separator plates in the MCFC. Four different conditions can be distinguished: MCFC cathode–gas at open circuit potential (OCP), cathode gas at MCFC load-conditions, anode gas at load conditions, and anode gas at OCP. In order to find a lifetime corrosion protective coating, the corrosion behaviour of the coatings has to be characterized and the corrosion rates of the coated samples have to be determined. The corrosion behaviour was characterized with cyclic voltammetry. Corrosion rates were calculated from measured corrosion currents and determined with cross-section analyses of corrosion layers. Corrosion currents were determined using amperometry and Tafel-extrapolation of quasi-stationary polarization-curve measurements. However, care should be taken in drawing conclusions only from measured currents, because it is difficult to separate corrosion currents from contributions of either the MCFC anode–gas reaction:

$$\tfrac{1}{2}H_2 + \tfrac{1}{2}CO_3^{2-} \leftrightarrow \tfrac{1}{2}H_2O + \tfrac{1}{2}CO_2 + e^- \quad (1)$$

under anode gas or the MCFC cathode-gas reaction:

$$\tfrac{1}{2}O_2 + CO_2 + 2e^- \leftrightarrow CO_3^{2-} \quad (2)$$

under cathode gas. Assuming that the measured current is only from the corrosion reaction, and that the coating oxidises to a solid scale which does not dissolve, a corrosion layer thickness or corrosion depth can be estimated from the current density. From the passed charge, which is given by the current density (i) integrated over the exposure time (t), a corrosion layer thickness or corrosion depth (D) can be estimated according to the equation:

$$D = \frac{M}{zF\rho}\int_0^t i\,\mathrm{d}t \quad (3)$$

in which F is the faradaic constant. The corrosion layer thickness can be estimated by assuming Li_2TiO_3 as main corrosion product, and using oxidation to tetravalent metal ions ($z = 4$), an average molar weight (M) of 110 g mol^{-1} [8], and a density (ρ) of 3.5 kg dm^{-3} [9]. The corrosion depth is equal to the corrosion layer thickness divided by factor 2.5 (using $z = 4$, $M_{TiN} =$ 62 g mol^{-1}, and $\rho_{TiN} = 5$ kg dm^{-3} [8]).

2. Coating deposition

Using different reactors, reactants, and deposition parameters, coatings differing in composition and morphology were prepared. The process parameters used during the deposition of the different coatings and the coating characteristics have been described earlier [2, 10]. For the thermally activated CVD of TiN or TiC, by using $TiCl_4$ with N_2 or CH_4 as precursors, deposition temperatures of over 900 °C are necessary [6]. Stainless steel 304 was chosen as substrate material because it is a (relatively cheap) austenitic steel. Austenitic steels do not show a phase transformation between room temperature and 1000 °C, whereas the used deposition temperature is too high for common steel substrates. The TiCN coatings labelled TiN–T3, TiN–T5, and TiC–T2 were deposited by using $TiCl_4$, N_2, CH_4, and H_2 as reactants. With metal organic precursors like tetrakis(dimethylamido) titanium (TDMAT) or tetraisopropoxytitanium (TTIP), lower deposition temperatures can be used. Using TTIP, a TiO coating labelled TiO–T1 was deposited at about 300 °C. TiO can be converted to TiO_2 rutile easily by two hours annealing at 450 °C in air. Rutile may have better corrosion protective properties than TiO. However, rutile is an electronic insulator, whereas TiO has a metallic conductivity. Therefore, the TiO-coated samples were not annealed before the electrochemical corrosion experiments. Also the use of a plasma allows lower deposition temperatures. A TiN coating labelled TiN–DC was deposited at 425 °C using TDMAT as precursor and a pulsed d.c.-plasma [11, 12].

The stainless steel 304 substrates were cleaned in ultrasonic baths successively with acetone and ethanol. To increase the coating-substrate adhesion, the substrate surfaces were etched with hydrogen before the plasma deposition [13, 14]. Preceding the thermal CVD, the substrate surfaces were etched with $TiCl_4$ and hydrogen. This results in thin intermediate layers of Ti [15–17] or TiC for carbon rich substrates [18], which are supposed to improve the coating–substrate adhesion, and improve the corrosion protective properties of TiN-coatings especially at small pores in the coating. The composition of the deposited coatings was analysed with energy dispersed X-ray analysis (EDX), the lattice parameter with X-ray diffraction (XRD), and the layer thickness was determined from cross sections with scanning electron microscopy (SEM) or light microscopy. Table 1 presents the characteristics of the different coatings (composition, layer thickness, lattice parameter, and colour).

Table 1. Characteristics of the different coatings

Sample batch	Composition (EDX)	Thickness /μm	Lattice parameter/Å	Colour	Details
TiN–T3	$TiN_{0.52}$	3.3	4.23	gold	multilayer of cubic TiN and N-deficient Ti_2N/TiN
TiN–T5	$TiN_{0.81}$	1.5	4.24	gold–brown	cubic TiN
TiN–Ph	$TiN_{0.82}$	2.8	4.23	gold	cubic TiN, surface with pinholes
TiN–DC	$TiN_{0.7}C_{0.3}$	2.9	4.21	light bronze	relatively-porous cubic TiCN
TiC–T2	$TiC_{0.67}$	2.8	4.33	black	cubic TiC
TiO–T1	TiO	0.62	3.59	blue–green	cubic TiO, thin
Ni	Ni	1.1	3.58	light grey	
Au	Au	3.0	–	gold	

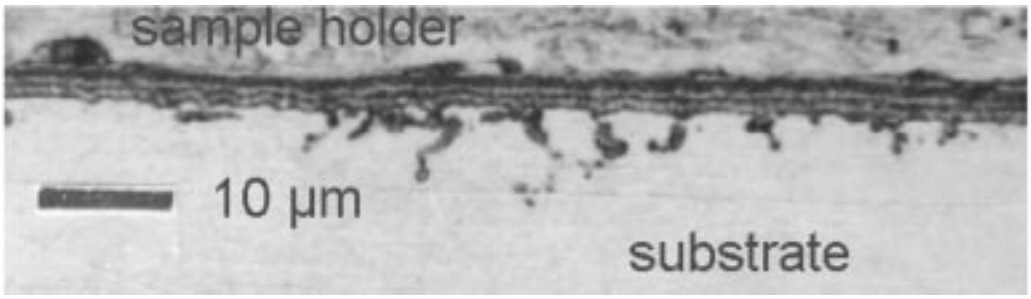

Fig. 1. Light-microscopy micrograph of a cross-section of the deposited TiN–T3 layer.

Figure 1 presents a micrograph of a cross section of the multilayered TiN–T3 coating. It shows dark TiC layers and light TiN-rich layers. The TiN layers were a mixture of cubic TiN Osbornite [19], tetragonal Ti_2N 12U [20], and tetragonal Ti_2N 6T [21]. The Figure also presents etching holes filled with chromium carbide. The TiN–DC-coating was a mixture of cubic TiN Osbornite and cubic TiC. The XRD peaks of this TiN–DC-coating were broad, which was probably mainly due to the formation of small crystals, and also due to carbon contamination from the TDMAT [22–26] in the form of TiC. The formation of small crystals might be due to gas-phase nucleation, and may have led to a relatively porous coating structure with many grain boundaries. The double-layer coatings were prepared by either sputtering nickel or by electrodeposition of gold on TiN–Ph-coated steel samples. The other coatings were all single layers of only one phase. The TiN coating labelled TiN–Ph was deposited by Philips in Eindhoven with thermal CVD. Surface analyses with atomic force microscopy showed in the TiN–Ph-coating surface some pinholes with a diameter of about 3.5 μm, which might be as deep as the whole coating.

3. Experimental aspects of corrosion experiments

Corrosion tests were performed in pot cells as shown in [1] at 650 °C in a melt of 62 mol % Li_2CO_3 and 38 mol % K_2CO_3 with MCFC–cathode or anode gas. The cathode gas consisted of 15% O_2, 30% CO_2, and 55% N_2. The anode gas consisted of 20% CO_2 and 80% H_2. The cathode gas was humidified at room temperature and the anode gas was humidified at 60 °C by feeding the gas through water at the indicated temperature. The outlet gas was led through a water lock to prevent air inlet. A reference electrode was used which comprised a gold wire immersed in the melt with standard reference gas (33.3% O_2, 66.7% CO_2). All potentials given are referred to this reference electrode. Under load, a potential of −950 mV was applied under anode gas and a potential of −100 mV was applied under cathode gas. These applied potentials correspond to the operating potentials under load in the MCFC [27].

The coated steel samples (surface area about 1 cm^2) were spot welded to a gold wire (0.5 mm dia., purity 99.9%) and cleaned with ethanol before the corrosion measurements, in which the samples were fully immersed in the melt. Corrosion currents were determined by amperometry and Tafel-extrapolation of quasi-stationary state polarization curves. The corrosion behaviour of the coated samples was characterised using potentiometry and cyclic voltammetry. For the electrochemical measurements an Eco Chemie Autolab-Pgstat20 controlled with an IBM-computer running the General Purpose Electrochemical System version 4 software was used. With cross-section analysis the thickness of the remaining coating and the thickness, structure, and composition of the corrosion layers were analysed with light microscopy, SEM, EDX and XRD. Before the analysis of the corrosion layers, the carbonate adhering to the samples was removed by rinsing in demineralized water.

4. Results and discussion corrosion experiments

4.1. *Cyclic voltammetry*

Cyclic voltammograms were measured between −1600 and +50 mV. The sweep rate was 50 mV s^{-1}, the scan increment was 10 mV, and the step time was 0.2 s. At load conditions corrosion of 304 steel was most severe under anode gas [2, 7]. Therefore, the corrosion behaviour of coated samples was studied with cyclic voltammetry under anode gas. However, besides the reactions of the coating material, these cyclic voltammograms also present reactions of the substrate material and the MCFC anode–gas reaction. Figure 2(a) presents the MCFC anode–gas reaction (Reaction 1, peak B) in a cyclic voltammogram measured on a gold-flag electrode. Gold is considered inert in molten carbonates. The corrosion behaviour of the substrate material, stainless steel 304 was described extensively in earlier publications [2, 7]. Figure 2(b) presents cyclic voltammograms measured on 304 steel, the substrate material. Figures 2(c)–(g) present cyclic voltammograms of five different coated samples: TiN–T3, TiN–T5, TiN–Ph, TiO–T1, and TiC–T2-coated steel. Figure 2(h) presents a cyclic voltammogram measured on an electrode of Li_2TiO_3, which is considered as the main corrosion product of the Ti-based coatings.

Porous Li_2TiO_3 electrodes were prepared by pressing Li_2TiO_3 powder into pellets. In these pellets a hole was drilled for a gold lead wire (0.5 mm dia.). The Li_2TiO_3 pellets were sintered at 1000 °C for 24 h and exposed to the molten carbonate under anode gas for at least 24 h before the cyclic voltammetry experiments. Although the samples turned from white to black and showed a large weight and volume increase of 18 and 3.6% respectively, no significant changes of the Li_2TiO_3 lattice parameters were detected. The Li_2TiO_3 had a monoclinic structure [28] with as lattice parameters: $a = 5.06$ Å, $b = 8.80$ Å, $c = 9.75$ Å, and $\beta = 100.3°$. The relative density (actual density divided by theoretical density) of the Li_2TiO_3 sample was 38%. The blackening and weight and volume increase of the Li_2TiO_3 sample can be due to a reduction reaction under influence of the reducing gas atmosphere. Hence, the oxidation of hydrogen gas (Reaction 1) at small anodic overpotentials of −1.1 V (against reference) at the

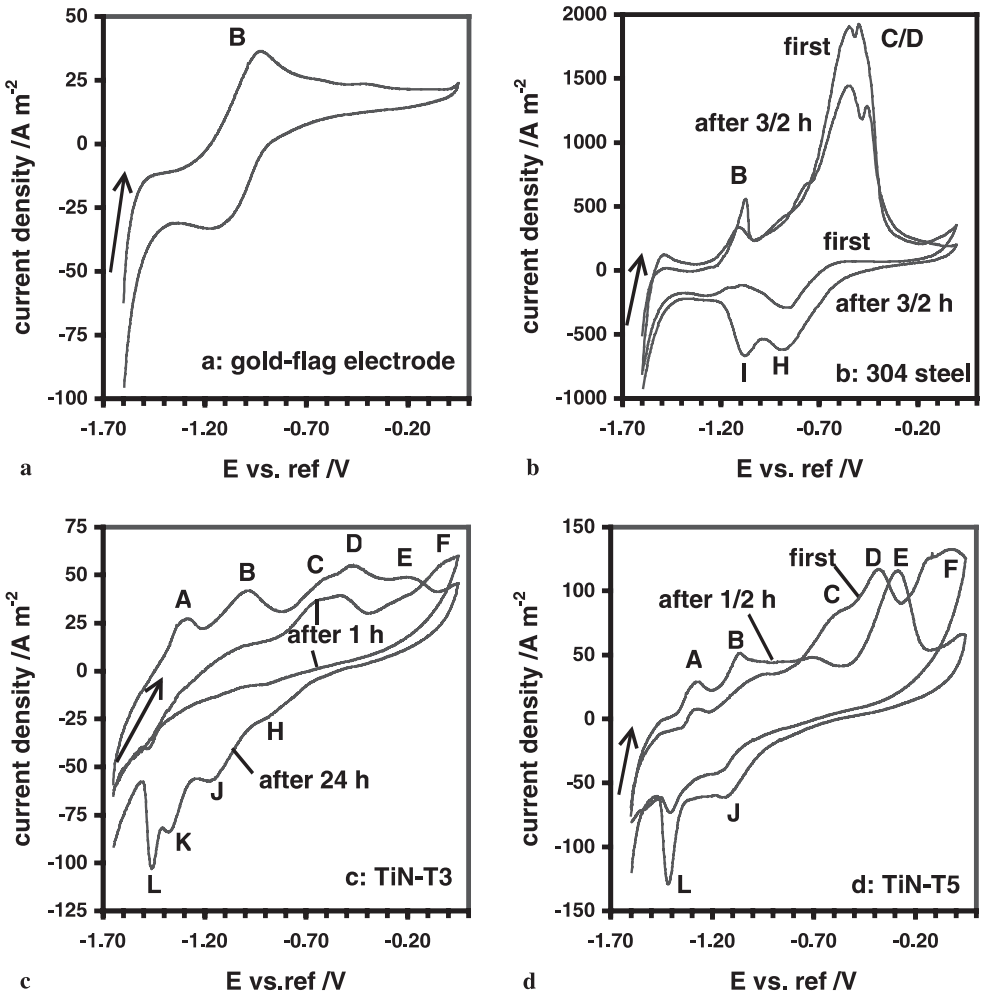

Fig. 2. Cyclic voltammograms on a gold flag (a), on 304 steel (b), TiN–T3 (c), TiN–T5 (d), TiN–Ph (e), TiO–T1 (f), TiC–T2-coated steel (g) and on Li_2TiO_3 (h) in molten carbonate under anode gas.

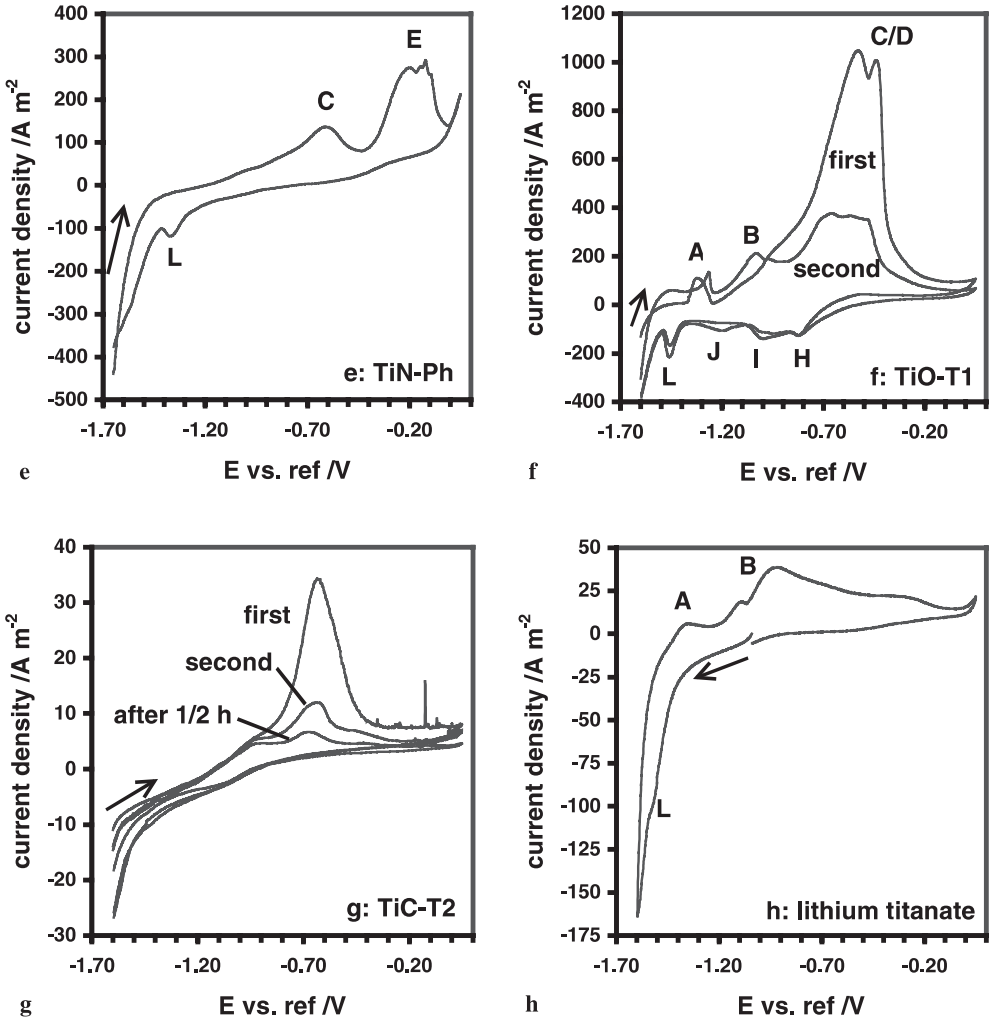

Fig. 2. Continued.

Li_2TiO_3 sample surface can lead to the reduction of tetravalent to trivalent titanium as written in defect-chemical Kröger–Vink notation:

$$Ti_{Ti}^{x} + e^{I} \leftrightarrow Ti_{Ti}^{I} \quad (4)$$

The sample blackening can be the result of free or trapped electrons Ti_{Ti}^{I} in the Li_2TiO_3 structure. To retain electroneutrality, the uptake of electrons resulting from the hydrogen oxidation reaction is accompanied with the interstitial insertion of lithium ions from the melt:

$$Li_{sol}^{+} + V_{i}^{x} \leftrightarrow Li_{i}^{\cdot} \quad (5)$$

The uptake of lithium ions results in a weight increase and gives, together with the titanium reduction, tensions in the structure leading to an increased volume and porosity. The carbonate adhering to the sample surface contributes to some extent to the weight increase.

From the current density in the cyclic voltammetry experiments, a rough estimate of the corrosion protection of the different coatings can be made. The current density for the TiN and TiC-coated samples is much lower than that for stainless steel, which indicates a much slower corrosion rate than that of steel and indicates corrosion protective properties. The TiO–T1-coated sample shows high current densities, indicating fast corrosion and no protection.

Further, a comparison of the corrosion protective properties of the different coatings has to be made. When the characteristics of steel become visible in the cyclic voltammogram, the corrosion protective properties of the coating have come to an end. Therefore, the first cycle measured just after immersion on the TiO–T1-coated steel indicates that this coating shows hardly any corrosion protection. The anodic peaks C and D in Figure 2(b) represent oxidations of iron, nickel, and chromium [2, 7]. Polarization of TiN–Ph samples at −0.6 V (peak C) gave iron oxides on the sample surface within one hour of exposure. Hence, also for TiN-coated samples peak C can represent oxidation of the substrate. The TiN–Ph coatings showed some pinholes, so a high C peak in the first cycle may be related to a high number of pinholes in the coating. The cathodic peaks H and I in Figure 2(b) can represent reductions of iron and nickel [2, 7]. After many cycles, these H and I peaks were also visible in the cycles on the TiN-coated steel, which indicates degradation during cycling.

Finally, the different peaks indicated by capitals in Figure 2(c) need to be assigned to reactions of the coating material. Anodic peaks from oxidation reactions of the coating material are expected. The TiCN and TiO coatings may oxidize to $LiTiO_2$ and further to Li_2TiO_3, or directly to Li_2TiO_3. However, it is not possible to assign with certainty one of the peaks C, D, E or F to one of these oxidations only from the present cyclic voltammetry experiments. The peaks A, B, J and L correspond with certainty to oxidation and reduction reactions of titanium, because these peaks were only visible with Ti-based materials. The anodic peak A was visible on the TiN and TiO-coated samples. At the OCP of about −1.0 V, the tetravalent titanium in Li_2TiO_3 is considered partly reduced to trivalent titanium. Therefore, peak A presents probably an oxidation towards trivalent titanium. Peak A measured in the first cycle on TiO–T1-coated steel was relatively large. For the TiN–Ph-coated samples, peak A arises only after the cathodic peak L. Therefore, peak A may be oxidation of the reduction product which was formed during peak L. The cathodic peaks J and L arise only after polarization anodically from peak B. A titanium valence higher than four is not expected. Therefore, peak B may indicate the oxidation of trivalent titanium to tetravalent titanium. This kind of titanium oxidation was also suggested by Okuyama [29]. To complete the circle, peak J represents the reduction of tetravalent to trivalent titanium, peak L the reduction of trivalent to bivalent titanium, and peak A the oxidation of bivalent to trivalent titanium. Polarization at the peak potential of peak E increases the height of peak L and J. Hence, peak E may be due to the oxidation of TiN to tetravalent titanium:

$$\tfrac{1}{2}\mathrm{TiN} + \tfrac{1}{2}\mathrm{Li_2CO_3} + \mathrm{CO_3^{2-}} \rightarrow \tfrac{1}{2}\mathrm{Li_2O.TiO_2} + \tfrac{1}{4}\mathrm{N_2} + 1\tfrac{1}{2}\,\mathrm{CO_2} + 2\,\mathrm{e^-} \quad (6)$$

$E^\circ = -1597$ mV (anode gas) or −1522 mV (cathode gas) calculated with data from [30]

Peak K was only visible on the TiN–T3-coated sample measured in the last cycle after 24 h of exposure. This shoulder K can not yet be explained. Using the Kröger–Vink defect notation and considering Li_2TiO_3 as main phase, peak A, B, J and L can be assigned to the following:

$$\mathrm{A} \quad \mathrm{Ti_{Ti}^{II}} \leftrightarrow \mathrm{Ti_{Ti}^{I}} + \mathrm{e^I} \quad (7)$$

$$\mathrm{B} \quad \mathrm{Ti_{Ti}^{I}} \leftrightarrow \mathrm{Ti_{Ti}^{\mathit{x}}} + \mathrm{e^I} \quad (8)$$

$$\mathrm{J} \quad \mathrm{Ti_{Ti}^{\mathit{x}}} + \mathrm{e^I} \leftrightarrow \mathrm{Ti_{Ti}^{I}} \quad (9)$$

$$\mathrm{L} \quad \mathrm{Ti_{Ti}^{I}} + \mathrm{e^I} \leftrightarrow \mathrm{Ti_{Ti}^{II}} \quad (10)$$

The corrosion behaviour of the coatings was then studied at the four different conditions. Table 2 presents the thickness of the remaining coating after exposure and Table 3 presents the corrosion layer thickness as determined from cross-section analysis of corrosion layers on coated and bare steel samples after 24 h of exposure. Table 4 presents the current density measured at different conditions.

4.2. *Corrosion under cathode gas at open circuit conditions*

First the corrosion behaviour of the different coatings under cathode gas was characterized by potentiometry by measuring the OCP during 24 h of exposure. Figure 3 shows four measurements: three of coated samples and one of gold, also called the gold-flag potential (GFP). The OCP is a mixed potential resulting from the MCFC cathode–gas reaction and possible

Table 2. Remaining coating thickness/μm after 24 h of exposure as determined with SEM or light microscopy analysis

Coating	Anode OCP	Anode −0.95 V	Cathode −0.1 V	Cathode OCP
TiN–T3	3.2	1.7	2.6	3.1
TiN–T5	2.3	none	none	2.0
TiN–Ph	2.7	2.5	1.8	1.2
TiN–DC	none	none	none	none
TiC–T2	none	none	none	1.0
TiO–T1	none	none	none	none
Ni	Ni particles	Ni particles	–	–
Au	–	–	gold particles	gold particles

Table 3. Corrosion layer thickness/μm on bare and coated 304 steel after 24 h/1 month of exposure determined with SEM or light microscopy analysis

Coating	24 h/1 month			
	Anode OCP	Anode −0.95 V	Cathode −0.1 V	Cathode OCP
None	5	14	3	20
TiN–T3	0.2/2	1.5/112	0.4/4.2	0.7/22
TiN–T5	0.5	22	7.8	3.1
TiN–Ph	0.4	3.8/92	1.9	1.2
TiN–DC	2.4	10/28	4.7	24
TiC–T2	14	18	7.6	5.0
TiO–T1	3.6	7.1	4.5	6.9

Table 4. Current density averaged over 24 h of exposure

Coating	Anode GFP	Anode −0.95 V	Cathode −0.1 V
None	0.50	6.0	0.69
TiN–T3	0.055	0.75	0.97
TiN–T5	−0.43	5.3	0.99
TiN–Ph	0.087	6.2	3.9
TiN–DC	0.75	5.6	0.97
TiC–T2	4.8	5.5	9.3
TiO–T1	0.42	0.47	4.5
Ni	−0.87	1.5	–
Au	–	–	8.6

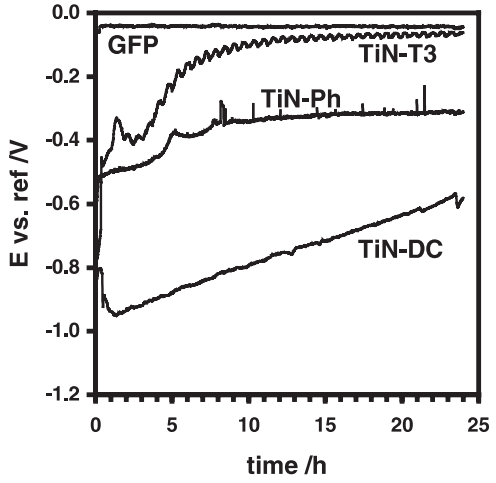

Fig. 3. OCP of coated steel against time under cathode gas.

corrosion reactions. The OCP of a noncorroding electrode (gold) is equal to the GFP. All samples showed an anodic potential shift towards the GFP. This presents the decreasing contribution of corrosion reactions to the measured OCP and passivation of the samples. The potential shifts occur with different time scales. A large potential difference between the GFP and the OCP appeared to be correlated to a thick corrosion layer.

Figure 4 shows a cross-section of the corrosion layer on the TiN–T3-coated sample after 30 days exposure. This Figure shows three corrosion layers which are characteristic for Ti-based coatings. EDX analysis of the top layer gave Fe and O as main elements. Therefore, the two peaks in the XRD spectrum of the sample surface were assigned to the [200] and [220] peaks of lithium ferrite ($LiFeO_2$) with a lattice parameter of 4.14 Å. EDX analyses of the two inner corrosion layers showed a Ti–Cr–Fe-oxide layer between the outer $LiFeO_2$ layer and the inner Cr–Fe-oxide layer.

Several coatings showed (almost) no Ti remainings after 24 h of exposure. This is probably due to the dissolution of titanate ions (TiO_3^{2-}) in the melt [31]. Ti

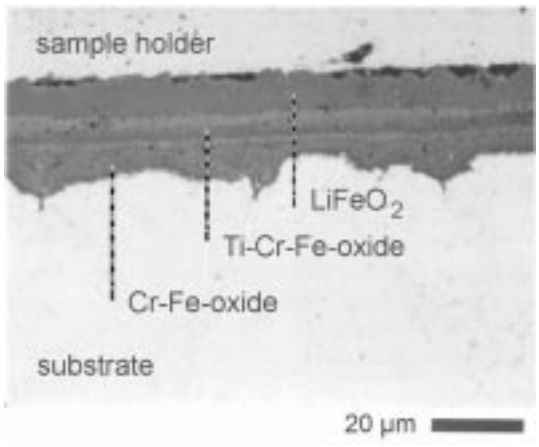

Fig. 4. Light microscopy cross section of TiN–T3-coated steel after 30 days of exposure under cathode gas at OCP.

was only found in corrosion layers as intermediate oxide or mixed oxide layer [29] with Fe and Cr between an outer $LiFeO_2$ layer and an inner Cr-enriched oxide layer. This presents the corrosion mechanism. The oxygen reduction at the sample surface:

$$\tfrac{3}{2}O_2 + 2\,Li^+_{sol} \leftrightarrow 3\,O^x_o + 2\,Li^x_{Li} + V^{IIII}_{Ti} + 6\,h^{\cdot} \qquad (11)$$

is accompanied with the absorption of lithium ions from the melt and the creation of titanium vacancies and electron holes. Holes are easily transported away from the surface in a p-type conductor as Li_2TiO_3. In order to balance this charge transport, metal ions are transported towards the sample surface and fill the titanium vacancies at the surface. After corrosion of the Ti-based coating, this process continues with iron ions from the substrate creating a $LiFeO_2$ layer on top of the Li_2TiO_3 layer. The corrosion layer formed underneath the Li_2TiO_3 layer can only be due to diffusion of oxygen along the grain boundaries. The diffusion of Fe ions is much faster than that of Cr or Ni, which leads to an Fe depleted or Cr and Ni-enriched inner corrosion layer.

With SEM analysis the surface structure was studied of the Au-coated sample (TiN–Ph-coated steel with a top layer of gold) after 24 h of exposure. The surface showed many small round gold particles (about 1.5 μm dia.), a corroded TiN-sample surface, and an accumulation of gold on the sample edges. Hence, the gold coating broke up into small particles and the coating showed a low adherence with the underlying TiN-coating.

Except for the TiN–DC-coated steel sample, the corrosion layer on the coated samples was much thinner than the corrosion layer on bare 304 steel after 24 h of exposure. Hence, all coatings, except the TiN–DC coating, protect against corrosion at these conditions for at least one day. The TiN–T3-coating showed the best corrosion protection. The sample showed almost no attack of the original coating and the thinnest corrosion layer. After 30 days exposure, the corrosion layer thickness on this sample is comparable with the thickness on bare 304 steel after only one day of exposure. The TiN–T3-coating retards corrosion of the underlying steel. Whether the protection lasts long enough depends on the length of time during which the fuel cell is off load.

4.3. *Corrosion under cathode gas at load conditions*

At load conditions (−100 mV), corrosion rates were determined from cross-section analyses of corrosion layers, and from the measured current density with amperometry. There is no clear relation between the corrosion layer thickness (Table 3) and the current density of the different coatings averaged over 24 h of exposure (Table 4). At −100 mV, the MCFC cathode–gas reaction gives a negative contribution to the measured current, which even leads to a negative value for the measured current after about 5 h of exposure for the TiN–

T3-coated steel, when the corrosion current becomes small due to passivation.

Most striking is that the measured current of the coated samples is, in all cases, higher than that of bare 304 steel, and that most corrosion layers were thicker than on bare 304 steel, except for TiN–T3 and TiN–Ph-coated steel. Possibly, bare 304 steel shows better passivation than most of the coated samples under these conditions. Only the coatings TiN–T3 and TiN–Ph were partly corroded after 24 h of exposure. Figure 5 shows that almost half of the originally 2.8 μm thick TiN–Ph-coating had corroded during 24 h of exposure. EDX measurements on cross-sections of the other coatings showed between the outer iron oxide and inner Cr–Fe-oxide layer, an intermediate Ti-containing oxide layer. The gold on the TiN coating was, similar to this sample exposed at OCP, coagulated on the sample edges after 24 h of exposure.

The TiN–T3-coating showed the best corrosion protection. The average current density of this coating corresponds with a corrosion layer thickness of 6.8 μm, which is much higher than the real value (0.4 μm). After 31 days of exposure, the TiN–T3-coated sample showed a scale of about 4.2 μm (Figure 6). EDX measurements on this sample showed that the TiN had been totally oxidised, no nitrogen was detected, and the steel substrate was not affected.

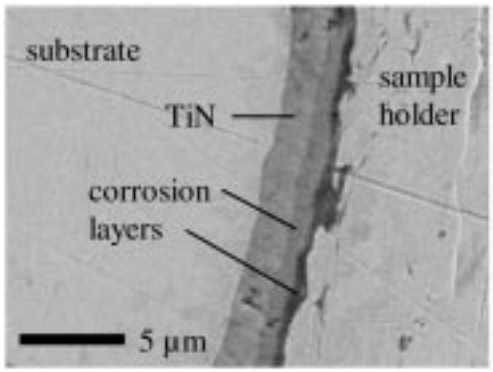

Fig. 5. SEM micrograph of a cross section of TiN–Ph-coated steel after 24 h of exposure under cathode gas at load.

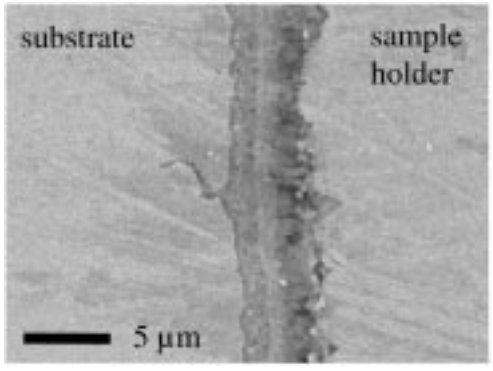

Fig. 6. SEM micrograph of a cross section of TiN–T3-coated steel after 31 days of exposure under cathode gas at load.

4.4. *Corrosion under anode gas at open circuit conditions*

The corrosion behaviour under anode gas was first characterized by potentiometry by measuring the OCP of the coated steel samples during 24 h of exposure. The OCP of the samples is a mixed potential resulting from the MCFC anode–gas reaction and possible corrosion reactions. The OCP of all samples was almost equal to the GFP. Hence, the contribution of the corrosion reaction to the OCP was probably small indicating slow corrosion. At the GFP, a corrosion current can be measured without contributing current of the MCFC anode–gas reaction, and which is representative for OCP conditions because the OCP almost equals the GFP. Corrosion rates were determined from cross-section analyses of corrosion layers, and estimated from corrosion currents determined with amperometry and with Tafel-extrapolation of quasi-stationary polarization curves.

Only the TiN–T3, TiN–T5, and TiN–Ph coatings showed remainings of the original coating after 24 h of exposure. For most coatings the corrosion layer thickness was less than that of 304 steel, except for the TiC–T2 coating. Hence, most coatings protect against corrosion at these conditions. The nickel layer on TiN–Ph coated steel was not stable and showed a similar behaviour as the gold layer on TiN-coated steel under cathode gas conditions. As shown in Figure 7, the Ni from the layer had coagulated to particles (about 1.5 μm dia.). EDX analysis showed partly oxidised TiN between the Ni-particles.

Quasi-stationary state polarization curves were measured for TiN–T3 coated steel between the OCP minus 0.25 V and the OCP plus 0.25 V after, respectively, 1, 2, 4, 8 and 24 h of exposure under anode gas. The sweep rate was 1 mV s^{-1}. The polarization resistance and, with the use of Tafel extrapolation, the current density were determined after different times of exposure as shown in Table 5. The OCP, polarization resistance, and corrosion current density all change slightly with increasing exposure time. The polarization resistance and corrosion current density change slightly with increasing

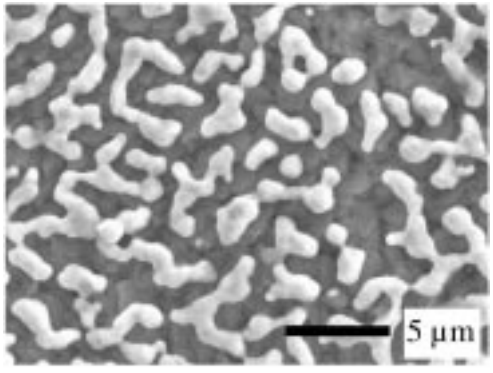

Fig. 7. SEM micrograph of the Ni-coated sample surface after 24 h of exposure under anode gas at OCP.

Table 5. Polarization resistance (R_p) and current density of TiN–T3-coated steel from quasi-stationary polarization measurements after different times of exposure under anode gas

Exposure/h	OCP/V	R_p/Ω	i/A m^{-2}
1	−1.079	200 ± 10	1.0
2	−1.082	225 ± 10	0.88
4	−1.083	224 ± 10	0.81
8	−1.092	241 ± 10	0.81
24	−1.108	170 ± 10	1.05

exposure time due to the growth of the corrosion layer and due to a changing surface activity for the hydrogen oxidation reaction. The corrosion layer thickness estimated from Tafel extrapolation (average current density 0.98 A m^{-2}) is 25 μm, which is much higher than the real value (0.2 μm). The estimated value is too high because of the contribution of the hydrogen oxidation reaction to the determined current. The corrosion layer thickness estimated from amperometry measurements (average current density 0.055 A m^{-2}) is 0.39 μm, which is higher than the real value.

The TiN–T3, TiN–T5, and TiN–Ph coatings showed the best corrosion protection at these conditions. The TiN–T3-coated samples showed no colour change after 24 h of exposure. After 31 days of exposure, they had turned black, but the thickness of the corrosion layer and remaining coating was still less than the corrosion layer thickness on bare steel after only one day of exposure.

4.5. *Corrosion under anode gas at load conditions*

Just as with the measurements under cathode gas at load, there seems to be no clear relation between the current density and the corrosion layer thickness. The corrosion layer thickness on TiN–T3-coated steel estimated from amperometry (average current density 0.75 A m^{-2}) is 5.3 μm, which is much thicker than the real value (1.5 μm). The Ni-coated sample showed after 24 h of exposure a similar surface structure as after 24 h at OCP (presented in Figure 7). Between the Ni-particles (about 1.5 μm dia.) partly oxidized TiN was visible.

After one month of exposure, the corrosion layer thickness on TiN–T3-coated steel was about 112 μm, about 88 μm on TiN–Ph-coated steel, and about 28 μm on TiN–DC-coated steel. All the coatings were completely corroded, and showed attack of the steel substrate after this relatively long exposure time. The corrosion layer thickness was expected to increase with the exposure time. However, from three investigated coatings, the coating with the thinnest corrosion layer after one day exposure (TiN–T3) showed the thickest corrosion layer after one month exposure. This makes it difficult to estimate the long-term behaviour of the different coatings. An explanation for this effect may be that the coating, which initially corrodes relatively slow, may form a relatively porous corrosion layer that protects less during long exposure times. Although these three coatings showed corrosion protection during one day of exposure, they are not good enough for lifetime corrosion protection in the MCFC.

4.6. *Comparison of corrosion protective properties and measurement methods*

The corrosion behaviour of several coated steel stamples was examined using cyclic voltammetry. High anodic peaks in the cyclic voltammograms indicate oxidation sensitive materials, and the corrosion protection is poor when the characteristic peaks of the steel substrate are visible. Therefore, the TiN and TiC coatings presented much better corrosion protective properties than the TiO coating.

Table 6 presents the corrosion layer thickness on TiN–T3 samples as estimated from corrosion current densities and determined from cross-section analyses of corrosion layers. Corrosion current densities were obtained by amperometry and with Tafel-extrapolation of quasi-stationary polarization curves. All the estimated values are too high compared to real values, which illustrates the low reliability of estimations of the corrosion layer thickness from corrosion current densities. Especially under anode gas at load, this difference can be attributed to a contributing current of either the MCFC anode–gas reaction under anode gas or the MCFC cathode–gas reaction under cathode gas to the measured current. The contribution may be different and change differently with increasing exposure time for different coated samples. Hence, a comparison of corrosion rates of different coated samples should not only be based on the measured corrosion currents.

Coatings differing in composition and morphology were tested at four different conditions, with emphasis on finding a relation between the coating composition, morphology, and corrosion properties. However, no clear relation was found between the coating characteristics and corrosion protective properties, partly because the investigated coatings differ from one another in more than one variable. Therefore, it is only possible to present the coating characteristics that have advantageous or disadvantageous effects on the corrosion protective properties of its coating:

(i) Layer thickness. The TiO–T1-coating was relatively thin (0.62 μm) compared with the other coatings (about 3 μm).

Table 6. Corrosion layer thickness/μm on TiN–T3-coated steel after 24 h of exposure determined with different methods

Method	OCP or GFP anode	−0.95 V anode	−0.1 V or GFP cathode	OCP cathode
SEM/light microscopy	0.2	1.5	0.4	0.7
Amperometry	0.39	5.3	6.8	
Tafel-extrapolation	25			

(ii) Pinholes. The TiN–Ph-coating surface showed some pinholes that might be as deep as the whole coating.
(iii) Density. The TiN–DC-coating was relatively porous. The TiN–T3-coating is probably more dense than the TiN–T5-coating, because it was deposited at a lower deposition temperature (in the surface reaction limited regime for CVD).
(iv) Composition. The TiO and TiC coatings appeared to be more sensitive for corrosion than TiN-based coatings. The TiN–DC-coating also contained some TiC, which gave this coating less corrosion protective properties than the other TiN-coatings. These results are in agreement with Arrando and Senna [32, 33], who found that the corrosion resistance of TiCN layers in aqueous media decreases with increasing carbon content.
(v) Passivation. The TiN-coatings always showed more remainings of the original coating than the TiC and TiO-coatings. Therefore, TiN has probably a better passivating capacity than TiC or TiO. The Ti-based coatings often form a mixed oxide layer with Fe and Cr between an outer $LiFeO_2$ and a Cr-enriched inner oxide layer. Hence, the intermediate Ti-layer does not form a sufficient barrier for the inward diffusion of oxygen and outward diffusion of Fe.
(vi) Stoichiometry. The TiN–T3-coating was a mixture of cubic substoichiometric TiN and two tetragonal Ti_2N-phases, whereas the other TiN-coatings had a higher stoichiometry and only the cubic phase. Although less corrosion protection is expected from substoichiometric coating materials, the TiN–T3-coating showed more corrosion protection than the other TiN-coatings. For the substoichiometric Ti_2N/TiN mixture literature suggests a superior wear protection and extreme hardness, but gives no information about the corrosion resistance compared with stoichiometric TiN [34].
(vii) Multilayers. The TiN–T3-coating was a multilayer of TiC and TiN/Ti_2N. The other coatings were single layers. The use of multilayers may increase the corrosion protection.

5. Conclusions

Five titanium carbonitride coatings differing in composition and morphology and a titanium monoxide coating were deposited by thermal and plasma-enhanced chemical vapour deposition. These coated samples were tested in molten carbonate, with emphasis on finding a relation between the coating composition, morphology and corrosion properties, and also in order to find a lifetime corrosion protective coating for separator plates in the MCFC.

These coatings were tested on their corrosion protection of stainless steel 304 separator plates in four different environments: under MCFC-cathode or anode gas, at load or at open circuit conditions. It was not possible to find a clear relation between the coating characteristics and corrosion protective properties at the four different conditions, partly because the investigated coatings differed from one another in more than one variable. It is only possible to present the coating characteristics that have advantageous or disadvantageous effects on the corrosion protective properties, for example, the coating thickness, density, composition, stoichiometry, the presence of pinholes or multilayers, and the passivating capacity of the coating. The titanium nitride coatings showed the best corrosion protection at all conditions, especially the TiN–T3-coating. The titanium carbide coating showed less protection and the thin titanium monoxide coating showed no corrosion protection at all.

The double-layer coatings of gold or nickel on a TiN-coating were not successful. The Au and Ni coatings broke up into small particles, which partly coagulated on the sample edges. Wind et al. [35] found that cladded Ni coatings were stable whereas electroplated Ni coatings were not. Possibly, the main reason for the stability of the cladded layer was its large thickness. Then a solution to this problem of unstable Ni and Au coatings on TiN might be to apply thick coatings (about 50 μm). A thick Ni or Au coating on top of a ceramic (TiN) coating might provide the necessary corrosion protection in molten carbonates.

As described earlier for stainless steel 304 [2, 7], the best corrosion protection under cathode gas conditions is given by keeping the cell at load. A TiN coating may give a further increase of the corrosion protection and may provide lifetime corrosion protection of the separator plates in the MCFC when kept at load. Under anode gas, the corrosion is most severe at load conditions as presented earlier for stainless steel 304 [2, 7]. Here, a TiN coating gives some corrosion protection. However, the coatings were not good enough for lifetime corrosion protection at load conditions. Hence, especially under anode gas at load conditions, a further search for corrosion protection is necessary.

References

1. M. Keijzer, K. Hemmes, P.J.J.M. van der Put, J.H.W. de Wit and J. Schoonman, *Corros. Sci.* **39** (1997) 483.
2. M. Keijzer, PhD thesis, 'Ceramic and metallic coatings for corrosion protection of separator plates in molten-carbonate fuel cells', Delft University of Technology, (1998).
3. V. Chauvaut, M. Cassir and Y. Denos, *Electrochim. Acta* **43** (1998) 1991.
4. V. Chauvaut, E. Duval, B. Malinowska, M. Cassir and P. Marcus, *J. Mater. Sci.* **34** (1999) 2015.
5. V. Chauvaut and M. Cassir, *J. Electroanal. Chem.* **474** (1999) 9.
6. J.P. Dekker, P.J. van der Put, H.J. Veringa and J. Schoonman, *J. Electrochem. Soc.* **141** (1994) 787.
7. M. Keijzer, G. Lindbergh, K. Hemmes, P.J.J.M. van der Put, J. Schoonman and J.H.W. de Wit, *J. Electrochem. Soc.* **146** (7) (1999) 2508.
8. R.C. Weast, 'Handbook of Chemistry and Physics', 56th edn, (CRC Press, Ohio, 1975/76).
9. JCPDS-card no. 8-249.

10. M. Keijzer, P.J.J.M. van der Put, J. Schoonman, S.F. Au, K. Hemmes and J.H.W. de Wit, *in* M.D. Allendorf and C. Bernard (Eds), *International Symposium on* 'Chemical Vapor Deposition', CVD XIV and EUROCVD 11, Vol. PV 97-25, 192nd Meeting of the Electrochemical Society, Paris, 31 Aug.–5 Sept. (1997), pp. 364–8.
11. J.P.A.M. Driessen, A.D. Kuypers and J. Schoonman, in L.A.J.L. Sarton and H.B. Zeedijk (Eds), *Proceedings of the 5th European Conferences on* 'Advanced Materials and Processes and Applications, Materials, Functionality and Design, Vol. 3, 'Surface Engineering and Functional Materials', EUROMAT, Maastricht, 21 Apr. (1997), p. 3/13.
12. J.P.A.M. Driessen, A.D. Kuypers and J. Schoonman, *Surf. Coat. Technol.* **110** (1998) 173.
13. K.-T. Rie, Th. Lampe and St. Eisenberg, *Härt. Tech. Mitt.* **42** (1987) 153.
14. F.H.M. Sanders, *Mat. Sci. Eng.* **A139** (1991) 85.
15. A.C. Agudelo, J.R. Gancedo, J.F. Marco and D. Hanžel, *J. Vac. Sci. Technol.* **A15** (1997) 3163.
16. S.J. Bull, P.R. Chalker, C.F. Ayres and D.S. Rickerby, *Mater. Sci. Eng.* **A139** (1991) 71.
17. R. Hübler, L. Alberts and G.K. Wolf, *Surf. Coat. Technol.* **60** (1993) 549.
18. M. Ürgen and A.F. Çakir, *Surf. Coat. Technol.* **96** (1997) 236.
19. JCPDS-card no. 38-1420.
20. JCPDS-card no. 23-1455.
21. JCPDS-card no. 17-386.
22. M.R. Hilton, G.J. Vandentop, M. Salmeron and G.A. Somorjai, *Thin Solid Films* **154** (1987) 377.
23. K. Ishihara, K. Yamazaki, H. Hamada, K. Kamisako and Y. Tarui, *Jpn. J. Appl. Phys.* **29**(10) (1990) 2103.
24. K.-T. Rie and A. Gebauer, *Mater. Sci. Eng.* **A139** (1991) 61.
25. K.-T. Rie, J. Wöhle and A. Gebauer, *Surf. Coat. Technol.* **59** (1993) 202.
26. Ch. Täschner, K. Bartsch and A. Leonhardt, *Surf. Coat. Technol.* **59** (1993) 207.
27. R.A. Donado, L.G. Marionowski, H.C. Maru and J.R. Selman, *J. Electrochem. Soc.* **140** (12) (1993) 3565.
28. JCPDS-card no. 33-831.
29. M. Okuyama, A. Tsurumi, Y. Itoi and S. Kambe, *Proceedings of the 11th International Corrosion Congress*, Florence, Vol. 4 (1990), 4.95.
30. M.W. Chase, C.A. Davies, J.R. Downey, D.J. Frurip, R.A. McDonald and A.N. Syverud, 'JANAF Thermodynamic Tables', 3rd edn, Vol. 14, suppl. no. 1, New York (1985).
31. G. Charlot and B. Trémillon, 'Chemical Reactions in Solvents and Melts' (Pergamon Press, Oxford, 1969) p. 496.
32. F. Arrando, M.C. Polo, P. Molera and J. Esteve, *Surf. Coat. Technol.* **68–69** (1994) 536.
33. L.F. Senna, C.A. Achete, T. Hirsch and F.L. Freire Jr., *Surf. Coat. Technol.* **94–95** (1997) 390.
34. J.-E. Sundgren and H.T.G. Hentzell, *J. Vac. Sci. Technol.* **A5**(5) (1986) 2259.
35. J. Wind, F. Nitschké and M. Meyer, *in* O. Savadogo and P.R. Roberge (Eds.), *Proceedings of the 2nd International Symposium on* 'New Materials for Fuel Cell and Modern Battery Systems', Montréal, Canada, 105 (1997).